

Article

Phenotyping Peanut Drought Stress with Aerial Remote-Sensing and Crop Index Data

Maria Balota ^{1,*}, Sayantan Sarkar ², Rebecca S. Bennett ³ and Mark D. Burow ^{4,5}

¹ Tidewater Agricultural Research and Extension Center, School of Plant and Environmental Sciences, Virginia Tech, Suffolk, VA 23437, USA

² Blackland Research and Extension Center, Texas A&M AgriLife Research, Temple, TX 76502, USA; sarkarsayantan@hotmail.com

³ United State Department of Agriculture-Agricultural Research Service, Stillwater, OK 74075, USA; rebecca.bennett@usda.gov

⁴ Texas A&M AgriLife Research, Lubbock, TX 79403, USA; mburow@tamu.edu

⁵ Department of Plant and Soil Science, Texas Tech University, Lubbock, TX 79409, USA

* Correspondence: mbalota@vt.edu

Abstract: Peanut (*Arachis hypogaea* L.) plants respond to drought stress through changes in morpho-physiological and agronomic characteristics that breeders can use to improve the drought tolerance of this crop. Although agronomic traits, such as plant height, lateral growth, and yield, are easily measured, they may have low heritability due to environmental dependencies, including the soil type and rainfall distribution. Morpho-physiological characteristics, which may have high heritability, allow for optimal genetic gain. However, they are challenging to measure accurately at the field scale, hindering the confident selection of drought-tolerant genotypes. To this end, aerial imagery collected from unmanned aerial vehicles (UAVs) may provide confident phenotyping of drought tolerance. We selected a subset of 28 accessions from the U.S. peanut mini-core germplasm collection for in-depth evaluation under well-watered (rainfed) and water-restricted conditions in 2018 and 2019. We measured morpho-physiological and agronomic characteristics manually and estimated them from aerially collected vegetation indices. The peanut genotype and water regime significantly ($p < 0.05$) affected all the plant characteristics (RCC, SLA, yield, etc.). Manual and aerial measurements correlated with r values ranging from 0.02 to 0.94 ($p < 0.05$), but aerially estimated traits had a higher broad sense heritability (H^2) than manual measurements. In particular, CO_2 assimilation, stomatal conductance, and transpiration rates were efficiently estimated (R^2 ranging from 0.76 to 0.86) from the vegetation indices, indicating that UAVs can be used to phenotype drought tolerance for genetic gains in peanut plants.

Keywords: mini-core; vegetation indices; color space indices; heritability



Citation: Balota, M.; Sarkar, S.; Bennett, R.S.; Burow, M.D. Phenotyping Peanut Drought Stress with Aerial Remote-Sensing and Crop Index Data. *Agriculture* **2024**, *14*, 565. <https://doi.org/10.3390/agriculture14040565>

Academic Editor: Jaime Prohens

Received: 7 March 2024

Revised: 25 March 2024

Accepted: 28 March 2024

Published: 2 April 2024



Copyright: © 2024 by the authors. Licensee MDPI, Basel, Switzerland. This article is an open access article distributed under the terms and conditions of the Creative Commons Attribution (CC BY) license (<https://creativecommons.org/licenses/by/4.0/>).

1. Introduction

Drought severely constrains peanut (*Arachis hypogaea* L.) production worldwide [1]. Reduced soil moisture during peanut flowering and pegging causes a severe reduction in the pod yield [2–9]. Drought stress reduces seed germination and vigor [8], impedes calcium (Ca) uptake [10,11], reduces nodulation and nitrate reductase activity [12,13], increases *Aspergillus flavus* mold contamination [14–16], and decreases oleic-to-linoleic fatty-acid ratios in seeds, which is detrimental to peanuts' shelf life and nutritional qualities [17]. Supplemental irrigation can ameliorate drought stress, but in the Virginia and Carolina (VC) production region, irrigation is available for less than 15% of the peanut acreage [18]. Under these conditions, drought-resilient peanut cultivars are needed, and previous studies have shown that breeding programs can improve this trait, using physiological characteristics [19–25]. For example, Rao et al. [26] showed that relative chlorophyll contents (RCCs) measured with a soil and plant analysis development (SPAD) chlorophyll

meter could be used to reliably identify genotypes with low specific leaf areas (SLAs) and high specific leaf nitrogen contents and that these traits were associated with improved transpiration efficiency in peanut plants [26]. In other legume crops, such as chickpeas, soybeans, lentils, and cowpeas, drought resulted in chlorophyll degradation and low stomatal conductance, leading to significant effects on the photosystem II (PS II) quantum yield and carbon assimilation and transpiration rates, thereby reducing crop yields [27,28]. Low stomatal conductance and subsequent reduced transpiration resulted in higher plant canopy temperatures [29].

Despite being useful in breeding, traditional methods for evaluating morpho-physiological characteristics associated with drought tolerance are slow and can only be used on a limited number of genotypes. In contrast, highly efficient remote-sensing techniques allow for hundreds of genotypes to be evaluated in a short period of time and reduce human error [30–32]. For example, in our program, the plant heights, leaf wilting, leaf area indices (LAIs), and lateral vine growths from 18 to 104 peanut genotypes were accurately estimated (84–99% accuracy) from aerial remote-sensing data [33–35].

The U.S. peanut mini-core collection with 112 accessions, including all the botanical and market peanut types, was selected from the core collection [36] by Holbrook and Dong (2005) [37]. The mini-core collection is an important germplasm source for improving drought tolerance, and, as a part of the National Institute of Food and Agriculture (NIFA), project # 2017-67013-26193, this collection was used to develop advanced molecular and physiological markers related to drought stress and rainfed production. Morpho-physiological evaluations were performed in New Mexico [38], Texas, Oklahoma, and Virginia [39], and molecular markers were developed (Burow, unpublished). To validate these markers and allow for in-depth phenotypic evaluation, a subset of 21 accessions exhibiting divergent phenotypes for traits associated with drought tolerance across these four states (data unpublished) and seven check genotypes were selected. In Virginia, the main objective was to assess these 28 genotypes for morpho-physiological traits (leaf wilting, canopy temperature, RCC, SLA, PS II quantum yield, and CO₂ assimilation rate (A); transpiration rate (E); stomatal conductance rate (g_s) and agronomic characteristics (pod yield, shelling percentage, and 100-seed weight) under late-season drought, imposed by rainout shelters, and well-watered conditions. The second objective was to identify accurate remote-sensing methods to estimate the morpho-physiological characteristics with high H² for accelerated phenotyping and increased yields under drought stress.

2. Materials and Methods

2.1. Plant Materials and Experimental Design

The experiments were performed at Virginia Tech's Tidewater Agricultural Research and Extension Center (TAREC) in Suffolk, VA (36.66498, −76.736569; 36.665139, −76.736682; 36.665304, −76.735875; 36.665464, −76.735982) on a Eunola soil type (fine-loamy, siliceous, thermic Aquic Hapludults). The twenty-eight peanut genotypes described previously were used in this study (Supplemental Table S1). These genotypes belong to the two subspecies of *Arachis hypogaea*, ssp. *hypogaea* and *fastigiata*, which have distinct morphological differences (*Hypogaea* has a shorter main stem and longer lateral branches than *fastigiata*) [40]. They were planted on 17 May 2018 and 30 April 2019, respectively, in double-row plots, 2.13 m long and 1.83 m wide at a seeding rate of 14 seeds m^{−2}. The design was a randomized complete block, with three replicates within each water regime, drought and well-watered. Each block was 21.3 m long by 7.3 m wide and separated by five peanut-border rows (4.75 m in total between the blocks). The land was tilled, and seedbeds were uniformly raised to 15 cm in height before planting. Cultivation practices recommended by the *Virginia Peanut Production Guide* were implemented [41]. The plots were rainfed until 8 weeks after planting (WAPs), after which rainout shelters were pulled over the drought regime plots. One rainout shelter was placed over each block or replicate on 16 July 2018 and 15 July 2019 to induce low soil moisture conditions. The rainout shelters were in place for 6 weeks before being removed on 30 August 2018 and 27 August 2019. The well-watered-regime plots

were rained throughout the season and because the rainfall from July through September in both years exceeded the multiannual average precipitation, supplemental irrigation was not needed. The rainfall, air temperature, and relative humidity (RH) were recorded daily from a weather station adjacent to the plots from 1 May until 30 September. Daily growing-degree days (GDD_{13s}) were calculated from the minimum and maximum daily temperatures, using a base temperature of 13 °C [42]. Only positive values were used; negative values were taken as 0, and temperatures above 35 °C were recorded as 35 °C.

2.2. Manual Data Collection

The canopy temperature depression (CTD) of each row was measured using an AGRI-THERM II™ (Model 100L) infrared thermometer. The “diff” option was selected, and the CTD value was calculated by subtracting the canopy temperature from the ambient air temperature. The CTD was measured over a random spot in each row, and values from two rows were averaged to obtain the plot’s CTD. Because the CTD is sensitive to wind and intermittent cloud covers, sunny days with minimal wind were selected for measurement. The CTD was measured from 6 WAPs until physiological maturity for a total of seven assessments per year.

Leaf wilting was visually assessed using the following 0–5 rating scale: 0, a healthy plant with no visible wilting or drooping leaves; 1, some terminal and newer leaves were folding but generally healthy overall; 2, upper leaves were almost all folded with visible signs of wilting, and lower and older leaves were starting to fold; 3, all the leaves were wilting and drooping on the plant, and some bare ground was becoming visible; 4, all the leaves were wilted and some were starting to change color due to chlorophyll degradation, bare ground was prominently visible, and some leaves were dead and dry; 5, all the leaves were severely wilted and from light green to yellow, bare ground was fully visible, more than 50% of the leaves were dead and dry, and the plant was almost physiologically dead [43]. Leaf wilting was measured from 6 WAPs until physiological maturity for a total of seven assessments per year.

The relative chlorophyll content (RCC) was measured using an SPAD meter sensor (SPAD-502, Minolta, Tokyo, Japan). Readings were taken from the third newest fully mature leaf on the main stems [26] of five randomly selected plants per plot. Care was taken to ensure that the meter sensor fully covered the lamina while avoiding interference from the leaf veins and midrib.

The specific leaf area (SLA) was calculated by dividing the leaf area by the leaf dry weight [44]. The five youngest, fully mature leaves were randomly selected from each plot, and the leaf area was measured using an LI-3100C area meter (LI-COR Biosciences, Lincoln, NE, USA). The same leaves were then dried in an incubator until the weight remained constant. The RCC and SLA from all 5 leaves of a plot were averaged. RCC and SLA measurements were taken at 10 and 14 WAPs in 2018 only.

The PS II quantum yield was measured using an OS30p+ plant stress meter (ADC BioScientific Ltd., Hoddesdon, UK). The device was used to measure the chlorophyll fluorescence from two dark- and light-adapted leaves from every plot. The photosystem II quantum yield refers to the efficiency with which photosystem II converts absorbed light energy to chemical energy during photosynthesis, whereas chlorophyll fluorescence is the emission of light by chlorophyll molecules when they are excited by light energy, providing insights into the photosystem’s activity [45]. For light-adapted readings, measurements were taken on fully illuminated leaves during the day from 10 a.m. to 3 p.m. For dark-adapted readings, an opaque clip was placed over the leaves and left for 30 min, so the reaction centers of PS II were fully reduced. The measurements included the maximal fluorescence with all the PS II reaction centers closed (F_m) and the minimal fluorescence with all the PS II reaction centers open (F_o). The difference between F_m and F_o is called the variable fluorescence (F_v). The F_v/F_m ratio is known as the PS II quantum yield and is an indicator for plant stress [46–49]. The PS II quantum yield was measured at 12 and 16 WAPs in 2019 only.

Gas exchange characteristics A , g_s , and E were measured with an LI6400 XT in 2018 and an LI6800 portable photosynthesis system in 2019 (LI-COR Biosciences, Lincoln, NE, USA). Readings were taken from two randomly chosen newest fully developed leaves on the main stem from each plot. The environment of the chamber was set at 2000 μmol of light, 50% relative humidity, 400 ppm of CO_2 , a 500 $\mu\text{mol s}^{-1}$ flow rate, and a 10,000 rpm mixing fan speed. The chamber's temperature was maintained to match the outside temperature. Leaves were clipped in the chamber for 60–90 s until the readings stabilized. Gas exchange measurements were taken at 14 and 16 WAPs in both years.

At physiological maturity, peanut pods were dug using a Sweere C200 peanut digger (Sweere Machinery, Oudenbosch, The Netherlands) and windrow-dried for approximately a week, and individual plots were combined using an Amadas 2110 two-row peanut combine. The pod yield was calculated once 7% seed moisture was obtained and after shelling; the shelling percentage and 100-seed weight from each plot were determined. The shelling percentage was calculated as the ratio of the seed to the pod weights multiplied by 100.

2.3. Aerial Data Collection

Each year, aerial images were taken before rainout shelters were installed (6, 7, and 8 WAPs) and after shelter removal (16 and 18 WAPs) to estimate the leaf reflectance, derived vegetation indices (VIs), and color space indices. An AscTec[®] Falcon 8 octocopter UAV platform (Ascending Technologies, Krailling, Germany) was used with a red–green–blue (RGB) (Sony[®] α 6000 digital camera, 24.3 megapixels (6000 \times 4000)) (Sony Corporation, Tokyo, Japan) and a near-infrared (NIR) camera (Tetracam[®] ADC micro, 3.2 megapixels, (2048 \times 1536)) (Tetracam Inc., Chatsworth, CA, USA). The flight campaign was in waypoint navigation, autopilot, and at 20 m altitude, with an image overlap of 75% forward and 90% sideways. Flight campaigns were created in AscTec[®] Navigator 3.4.5 software (Ascending Technologies, San Jose, Germany). A flight speed of 3 m/s was automatically adjusted by the navigator, based on the altitude and overlap. The flight campaign created by the navigator also created buffers all around the fields to have the maximum overlap. Therefore, a total of 0.22 Ha was covered by each flight campaign, taking 11 min to complete. At a 20 m altitude, the ground-sampling distance (GSD) was 0.6 cm for RGB and 0.55 cm for NIR sensors having a digitization footprint of 0.62 GB/Ha/band. The UAV's built-in GPS was used for navigation, acquiring nadir images, and recording individual images. All the flight campaigns were undertaken between 11 a.m. and 2 p.m. to be close to solar noon, and cloudy days were strictly avoided to prevent variation in the aerial imagery. Orthomosaic images were processed using Pix4Dmapper version 4.2.26 software (Prilly, Switzerland) to create RGB and NIR field maps. The 'reflectance map' option in the 'index calculator' step of Pix4D processing was used to create individual red, green, blue, and NIR reflectance maps.

The orthomosaic field maps were exported to the ArcMap tool (version 10.6) of ArcGIS (ESRI, Redlands, CA, USA). Polygons were drawn on the orthomosaic to outline each row (3.05 m long \times 0.9 m wide) and were numbered. Polygons were shifted to overlap the respective plot rows and collated into a single shapefile to create a fishnet. The fishnets were common for all the images from every flight campaign with georeferencing [31,32]. Georeferencing used the GPS coordinates of preinstalled ground control points (GCPs) in the field, covering the corners and central areas of the experimental plots. The zonal statistics option was used to extract the digital numbers (DNs) from each row. This process averaged the raster information of every pixel within each polygon to give the DN of red, green, and blue.

Calibration was performed using a reflectance panel with eight different shades from white to black [42]. The DN of the eight shades were recorded for red, green, blue, and NIR rasters from each orthomosaic. On the day of every flight, the reflectance from each of the eight shades of the panel were measured using an ASD HH2 hand-held VNIR spectroradiometer (Malvern Panalytical, Malvern, UK). The DN and reflectance from the

panel were fitted in exponential regression models. The models trained to derive reflectance values from DNs were as follows:

$$\text{red} = 0.1263 \times 1.0091^{\text{DN}_r}; \quad (1)$$

$$\text{green} = 0.1263 \times 1.0087^{\text{DN}_g}; \quad (2)$$

$$\text{blue} = 0.1144 \times 1.0087^{\text{DN}_b}; \quad (3)$$

$$\text{NIR} = 0.0563 \times 1.0147^{\text{DN}_n}; \quad (4)$$

where red, green, and blue are the reflectances from the respective rasters; and DN_r , DN_g , and DN_b are the digital numbers from red, green, and blue rasters, respectively. The reflectance values of both rows of each plot were averaged to obtain the average reflectance value of the plot.

The fishnet shapefile was also used to crop individual rows from every RGB ortho-mosaic, using ArcMap automatically. Images of individual peanut rows were used to extract 11 RGB color space indices using the BreedPix tool from the CIMMYT maize scanner 1.16 plugin (<http://github.com/george-haddad/CIMMYT> (accessed on 19 May 2018); Kefauver, S. C., University of Barcelona, Barcelona, Spain) produced as a part of the Image J/Fiji open-source software (<http://fiji.sc/Fiji> (accessed on 19 May 2018)) [50,51]. The color space indices extracted were intensity, hue, saturation, lightness, a^* , b^* , u^* , v^* , green area (GA), greener area (GGA), and crop senescence index (CSI) [52–57]. Indices a^* and u^* represent color shifts from green to red, and b^* and v^* from blue to yellow [34]. From the red, green, blue, and near-infrared reflectances, the following vegetation indices (VIs) were computed: normalized difference vegetation index (NDVI) [58], normalized plant pigment ratio (NPPR) [35], normalized green–red difference index (NGRDI) [59], plant pigment ratio (PPR) [60], and normalized chlorophyll pigment index (NCPI) [61]. These VIs range from -1 to $+1$, and they are highly sensitive to changes in leaf pigments and crop physiological traits [35].

2.4. Statistical Procedure

Data analyses were performed in Statistical Analysis System (SAS) version 9.4 (SAS Institute Inc., Cary, NC, USA). PROC GLM was used for analysis of variance (ANOVA). The measurements collected multiple times were analyzed as repeated-measures ANOVA using the “nouni” command and repeated option in PROC GLM. Fisher’s protected least significant difference (LSD) at $\alpha = 0.05$ was used for mean separation based on the number of levels in a particular factor. When the designs were unbalanced, the least-square means (LSmeans) mean separation procedure, adjusted for Student’s t test at $\alpha = 0.05$, was utilized. PROC CORR was employed for Pearson’s correlation analysis to evaluate the relationship between proximally and aerially collected data. The broad-sense heritability (H^2) was calculated as the ratio of the genotypic to phenotypic variances [62] and categorized as low ($<30\%$), medium (31–60%), and high ($>61\%$) [63]. PROC REG was used to perform multiple linear regressions and derive the models for A, g_s , and E from the VIs. Stepwise selection was performed using PROC GLMSELECT to select the best predictors for the models. The predicted residual error sum of squares (PRESS) statistic was used to determine the model’s efficiency from the coefficient of determination (the higher the R^2 , the better the model), root-mean-square error (RMSE), Akaike test criterion (AIC), Bayesian information criterion (BIC), and average square error (ASE) (lower RMSE, AIC, BIC, and ASE values are better). The PRESS option in the model statement was used to calculate all the model efficiency parameters. Graphs were built using JMP® Pro 15.0.0 (SAS Institute Inc., Cary, NC, USA).

3. Results and Discussion

3.1. Environmental Considerations

The temperature information along with the cumulative GDD_{13} and rainfall from 1 May to 30 September are reported in Figure 1. During the 2018 and 2019 growing seasons, the air

temperature was higher than the multiannual (30-year average) because of nighttime temperatures 10–15 °C above the 35-year average, rather than higher maximum daily temperatures (Figure 1). Consequently, the cumulative GDD₁₃ values exceeded the multiannual average in both years and were slightly higher under the rainout shelters. The cumulative rainfall was the highest in 2019, surpassing that of 2018 from early June to mid-August as well as the 35-year average from early June through the end of September. Inside the rainout shelters, the cumulative rainfall was 311 mm and 276 mm less than that outside the shelters in 2018 and 2019, respectively. The relative humidity (RH) differed significantly between the years. From the planting until mid-July, the RH in 2018 (80%) was nearly twice that in 2019 (ca. 40%). Also, the RH inside and outside the rainout shelters was similar from May to Sep in both years (Figure 1). In summary, 2018 was less favorable for optimal peanut production than 2019, with higher temperatures and RHs, and less rainfall during much of the peanut flowers' development. Similarly, inside the rainout shelters, plants had 35 mm less soil water available in 2018 in comparison with 2019. The variable weather encountered during this two-year study is typical for coastal Virginia [64]. Under these conditions, repeated-measures ANOVA showed no significant WAP × genotype interactions within each year and water regime except for RCC and SLA in both water regimes in 2018 and CTD under drought conditions in 2019, which was expected. Despite our efforts to measure only on sunny days with minimal wind, the CTD is highly dependent upon the ambient temperature and cloud cover at the time of the measurement [65]. The RCC and SLA are expected to change over the growing season and in response to the environmental effects. Because the emphasis in this study was on the overall genotypic response, the traits collected at multiple WAPs were averaged for factorial ANOVA.

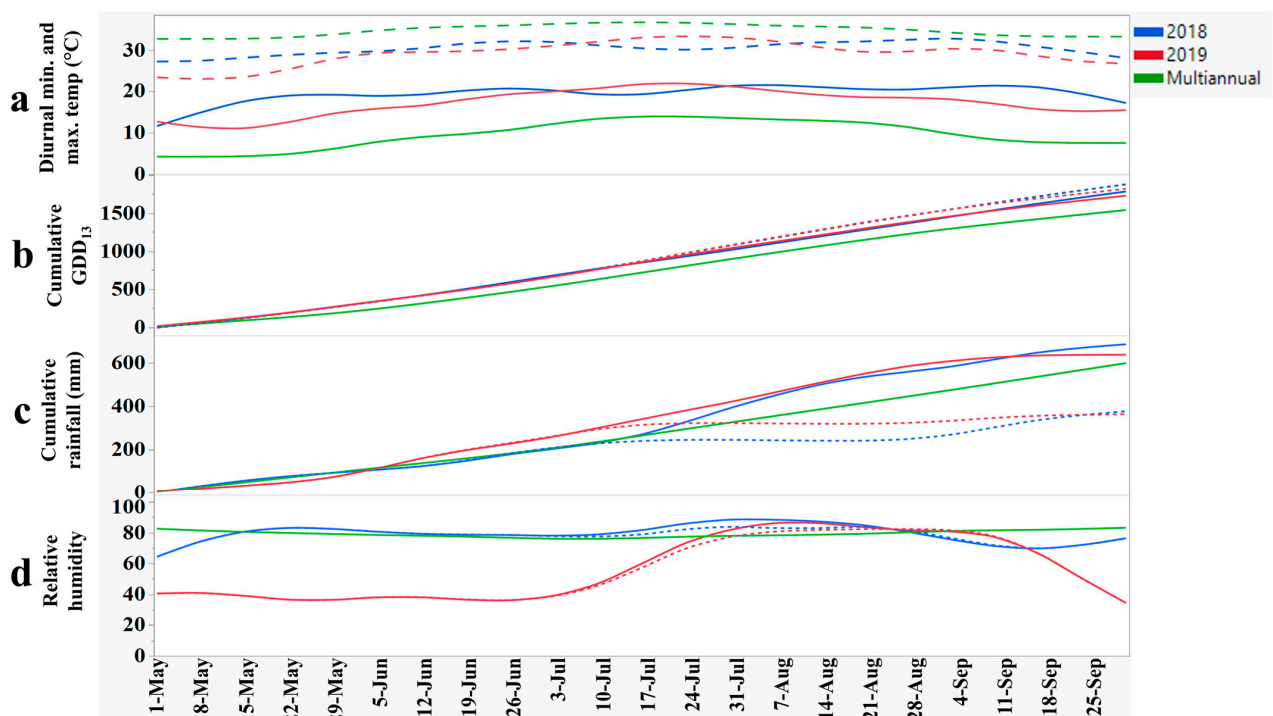


Figure 1. Weather data for the Tidewater region of Virginia, comprising (a) diurnal minima (solid lines) and maximum temperatures (dotted lines) (°C); (b) cumulative growing degree days (at 13 °C); (c) cumulative rainfall (mm); (d) relative humidity for 2018, 2019, and multiannual (1984–2019) average. The dotted lines in (b–d) are cumulative GDDs, rainfalls, and relative humidities inside the rainout shelters in contrast to the outside (solid lines).

Factorial ANOVA showed that the year, water regime, genotype, and their interactions had significant effects on manually measured morphological, physiological, and agronomic characteristics (Table 1). The effect of the year was significant ($p =$ from 0.045 to <0.0001)

for all the characteristics measured in both years except for the 100-seed weight. The water regime had significant ($p < 0.0001$) effects on all the characteristics except for the SLA and dark-adapted PS II. The dark-adapted PS II was affected by the water regime, however, at only a 10% probability. When years and water regimes were combined, the genotype had significant effects ($p =$ from 0.025 to <0.0001) on all the characteristics except for the light-adapted PS II quantum yield, CTD, A, E, and g_s . The interaction of $G \times E$ (year, water regime, or both) was not significant for the light- and dark-adapted PS II quantum yields, CTD, A, E, g_s , crop yield, shelling percentage, or 100-seed weight (Table 1). Among all the traits, only leaf wilting had a significant year \times water regime \times genotype interaction. The differences within the water regimes can be attributed to the physiological changes in the peanut plants because of drought stress. Higher disease occurrence in 2018 may explain the differences within these years. However, our primary objective was the differences among the genotypes. Therefore, we conducted mean separation for genotypes after stratifying them by water regime and year.

Table 1. Analysis of variance (ANOVA) of the morphological, physiological, and agronomic traits measured for 28 U.S. peanut mini-core and check genotypes grown in drought and well-watered regimes in 2018 and 2019. The year is missing for the RCC, SLA, and quantum yield because measurements for those were in one year only. Treatments within factors that have $p < 0.05$ are significantly different.

Source	RCC			SLA			Quantum Yield (Light)			Quantum Yield (Dark)		
	DF	F Ratio	p-Value	DF	F Ratio	p-Value	DF	F Ratio	p-Value	DF	F Ratio	p-Value
Water Regime (WR)	1	37.9	<0.0001	1	2.7	0.104	1	22.4	<0.0001	1	2.7	0.099
Block	2	5.9	0.003	2	12.5	<0.0001	2	0.5	0.621	2	1.3	0.264
Genotype (G)	27	7.8	<0.0001	27	2.1	0.003	27	1.3	0.149	27	1.7	0.025
WR \times G	27	2.1	0.003	27	1.7	0.018	27	1.0	0.414	27	0.7	0.871
Error	194			185			278			278		
	CTD			Wilting			Photosynthesis			Transpiration		
	DF	F ratio	p-Value	DF	F ratio	p-Value	DF	F ratio	p-Value	DF	F ratio	p-Value
Year	1	16.4	<0.0001	1	60.0	<0.0001	1	80.1	<0.0001	1	353.7	<0.0001
Water Regime (WR)	1	264.5	<0.0001	1	632.7	<0.0001	1	176.3	<0.0001	1	525.5	<0.0001
Block	2	0.9	0.426	2	23.8	<0.0001	2	0.4	0.687	2	2.7	0.069
Genotype (G)	27	0.6	0.950	27	2.5	<0.0001	27	0.8	0.800	27	0.9	0.681
Year \times G	27	0.7	0.833	27	1.0	0.497	27	0.5	0.986	27	0.3	0.999
WR \times G	27	0.7	0.860	27	1.1	0.279	27	0.2	1.000	27	0.2	1.000
Year \times WR \times G	27	0.6	0.949	27	1.5	0.038	27	0.2	1.000	27	0.3	1.000
Error	979			978			754			754		
	Stomatal Conductance			Pod Yield			Shelling (%)			100-Seed Wt.		
	DF	F ratio	p-Value	DF	F ratio	p-Value	DF	F ratio	p-Value	DF	F ratio	p-Value
Year	1	44.2	<0.0001	1	239.0	<0.0001	1	4.1	0.045	1	1.1	0.298
Water Regime (WR)	1	186.5	<0.0001	1	418.6	<0.0001	1	67.6	<0.0001	1	22.7	<0.0001
Block	2	1.1	0.349	2	0.8	0.455	2	4.6	0.011	2	0.2	0.796
Genotype (G)	27	0.7	0.839	27	3.8	<0.0001	27	6.2	<0.0001	27	10.5	<0.0001
Year \times G	27	0.4	0.996	27	1.4	0.090	27	1.6	0.046	27	11.2	<0.0001
WR \times G	27	0.4	0.997	27	0.8	0.749	27	1.9	0.006	27	1.3	0.191
Year \times WR \times G	27	0.5	0.991	27	1.0	0.515	27	1.2	0.253	27	1.1	0.335
Error	726			223			216			216		

DF—degree of freedom; CTD—canopy temperature depression; RCC—relative chlorophyll content; SLA—specific leaf area.

3.2. Morpho-Physiological and Agronomic Characteristics in Well-Watered Regime

The plant canopy is usually cooler than the air, and its temperature depends on the degree of stomata opening and the evaporative cooling of the plant, i.e., water availability [66,67]. The CTD, which is the difference between the canopy and air temperatures, is a known indicator of plants’ water status and response to drought and heat in various crops, including peanuts [64,68]. Under the well-watered conditions, the average CTD for the genotypes was -2.4 °C in 2018 and -3.1 °C in 2019, with all the genotypes showing cooler canopies compared to the air (Table 2). Consequently, little wilting (score < 1) was observed in most genotypes in the well-watered regime in both years. Moderate wilting (score < 3) was observed in New Mexico Valencia C PI 162655 and PI 339960 in 2018 and in PI 493938 in 2019.

Table 2. Growth and yield characteristics of 28 U.S. peanut mini-core and check genotypes grown under well-watered conditions in 2018 and 2019. The values followed by the same letters are not significantly different using LS means adjusted for Student’s *t* test at $\alpha = 0.05$.

Genotype	CTD (°C)		Wilting (0–5)		RCC	SLA (cm ² g ⁻¹)	PS II Quantum Yield (2019)		A (μmol m ⁻² s ⁻¹)		g _{sw} (mol m ⁻² s ⁻¹)		E (mmol m ⁻² s ⁻¹)		Pod Yield (kg ha ⁻¹)		Shelling (%)		100-Seed Weight (g)		
	2018	2019	2018	2019	2018	2018	Light	Dark	2018	2019	2018	2019	2018	2019	2018	2019	2018	2019	2018	2019	
Wynne	-3.2 a	-3.4 a	0	D	0.7 a	41.3 a	28.8 g	0.68 a	0.73 a	21.4 a,b	29.9 b-g	0.59 a	0.93 a	8.3 a,b	15.4 a	6276 a,b	6122 a	66.8 a	66.7 e-h	53.0 b-f	113.8 a
Walton	-1.8 a	-3.3 a	0	D	0.6 a	42.7 a	30.0 g	0.67 a	0.76 a	22.9 a	30.7 b-g	0.48 a-e	0.99 a	8.4 a,b	15.8 a	6915 a	6549 a	70.0 a	70.8 b-h	56.8 a-f	101.9 a,b
TVOL14	-0.1 a	-3.5 a	0.2	D	0.5 a	30.8 g	42.3 a-f	0.68 a	0.70 a	14.7 g-j	31.7 a-d	0.32 d-h	0.82 a	5.9 g-k	15.5 a	2425 d-g	5890 a	61.4 a	71.2 b-g	54.2 b-f	49.2 g-k
TS90	-2.5 a	-3.6 a	0	D	0.6 a	38.7 a-f	37.6 a-g	0.70 a	0.72 a	16.5 e-h	32.3 a-c	0.32 c-h	0.94 a	6.0 g-k	15.4 a	2702 d-g	4805 a	64.7 a	69.5 c-h	43.3 e,f	40.9 k-m
TROL11	-3.6 a	-3.2 a	0.3	cd	0.4 a	41.6 a	33.9 d-g	0.69 a	0.69 a	20.1 a-e	31.9 a-d	0.37 b-h	0.87 a	7.4 a-f	15.6 a	3260 c-f	4727 a	72.9 a	76.5 a,b	69.8 a-c	53.9 g-i
NMVALC	-1.4 a	-2.5 a	2.3 a	0.5 a	34.7 e-g	49.3 a	0.66 a	0.65 a	24.6 l	32.8 a,b	0.13 i	1.06 a	3.4 l	16.5 a	1628 g	6975 a	61.1 a	67.9 d-h	72.7 a,b	44.9 i-m	
PI 323268	-2.2 a	-3.7 a	0.3	d	0.3 a	41.0 a-c	34.4 d-g	0.68 a	0.70 a	21.3 a-c	33.2 a,b	0.49 a-d	1.01 a	8.0 a-c	16.7 a	3766 c-e	5464 a	61.0 a	66.9 e-h	66.0 a-d	71.5 d,e
PI 476636	-2.4 a	-3.9 a	0	d	0.5 a	42.4 a	44.8 a-e	0.69 a	0.73 a	16.6 e-h	31.7 a-d	0.31 e-h	0.89 a	6.1 f-j	16.3 a	3476 c-f	5386 a	66.7 a	71.2 b-g	51.7 b-f	55.2 g,h
PI 478819	-2.2 a	-3.3 a	0	d	0.3 a	38.1 a-f	37.7 a-g	0.70 a	0.70 a	17.5 c-h	32.0 a-d	0.37 b-h	0.86 a	6.8 c-h	15.9 a	2823 d-g	6006 a	.	80.6 a	49.8 c-f	67.3 e,f
PI 403813	-2.2 a	-2.6 a	0.8	b,c	0.6 a	38.5 a-f	46.6 a-c	0.67 a	0.68 a	16.3 e-h	27.7 f,g	0.41 a-h	0.75 a	6.8 c-i	13.4 a	2327 e-g	5076 a	59.9 a	70.0 b-h	63.5 a-d	40.0 l-n
PI 157542	-1.8 a	-2.7 a	0	d	0.6 a	37.9 a-f	34.4 d-g	0.68 a	0.68 a	20.6 a-d	32.2 a-d	0.57 a	0.99 a	8.7 a	16.1 a	2425 d-g	4960 a	67.8 a	71.9 b-f	81.0 a	42.9 j-m
PI 259836	-2.6 a	-2.6 a	0	d	0.6 a	33.3 f,g	43.2 a-e	0.69 a	0.70 a	18.5 b-g	31.6 a-d	0.40 a-h	0.94 a	7.7 a-d	15.8 a	2354 e-g	6122 a	64.8 a	72.2 b-e	42.8 f	44.8 i-m
PI 296558	-3.1 a	-3.8 a	0	d	0.6 a	40.9 a-d	31.1 f,g	0.68 a	0.74 a	16.1 f-i	30.8 b-f	0.35 c-h	1.03 a	6.5 d-i	15.2 a	3162 d-g	4650 a	68.9 a	70.1 b-h	61.4 a-e	81.9 cd
PI 319768	-2.7 a	-2.9 a	0.2	d	0.6 a	40.1 a-c	35.4 c-g	0.69 a	0.69 a	19.7 a-f	32.4 a-c	0.38 b-h	0.98 a	7.4 a-f	15.7 a	2977 d-g	4650 a	60.4 a	68.6 d-h	47.0 d-f	39.5 l-n
PI 268996	-2.0 a	-3.7 a	0	d	0.3 a	41.5 a	32.9 e-g	0.68 a	0.71 a	21.9 a,b	34.4 A	0.50 a-c	1.01 a	8.6 a,b	16.7 a	2932 d-g	5541 a	65.4 a	75.7 a-c	53.7 b-f	51.5 g-j
PI 162655	-2.7 a	-2.6 a	1.1	b	0.6 a	35.2 b-g	43.9 a-e	0.70 a	0.63 a	14.8 g-j	30.3 b-g	0.42 a-h	0.98 a	6.2 e-j	14.3 a	2867 d-g	4417 a	77.9 a	71.1 b-g	58.9 a-f	45.6 i-l
PI 298854	-2.4 a	-3.4 a	0	d	0.5 a	41.3 a	37.1 b-g	0.69 a	0.71 a	17.4 d-h	32.1 a-d	0.41 a-h	1.08 a	7.6 a-e	15.3 a	2456 d-g	6549 a	66.5 a	67.6 d-h	51.1 b-f	84.9 b-d
PI 343398	-2.4 a	-3.5 a	0	d	0.5 a	38.5 a-f	43.5 a-e	0.67 a	0.70 a	15.5 g-i	32.1 a-d	0.29 f-h	1.21 a	6.2 f-j	16.9 a	2538 d-g	6122 a	61.8 a	64.2 h	55.6 b-f	92.6 b,c
PI 290594	-2.6 a	-3.5 a	0	d	0.4 a	38.3 a-f	35.8 c-g	0.68 a	0.72 a	17.6 c-h	33.1 a,b	0.46 a-f	0.93 a	7.2 b-g	16.0 a	3324 c-f	6045 a	63.5 a	70.7 b-h	59.6 a-f	55.3 g,h
PI 274193	-2.3 a	-3.5 a	0	d	0.8 a	41.2 a,b	37.1 b-g	0.68 a	0.71 a	16.5 e-h	31.4 a-e	0.45 a-g	0.84 a	7.5 a-f	16.4 a	2111 f,g	5735 a	63.9 a	68.9 d-h	48.4 d-f	58.7 f,g
PI 339960	-2.6 a	-1.6 a	2.7 a	0.7 a	34.9 d-g	45.3 a-d	0.67 a	0.70 a	10.1 kl	29.0 d-g	0.36 c-h	0.91 a	4.6 kl	14.1 a	2146 f,g	5619 a	60.9 a	65.2 f-h	54.2 b-f	48.7 g-k	
PI 502120	-2.6 a	-2.6 a	0.3	cd	0.9 a	38.0 a-f	28.6 g	0.68 a	0.74 a	15.5 g-i	27.5 G	0.35 c-h	0.82 a	6.6 d-i	13.8 a	2890 d-g	6394 a	58.6 a	64.6 g,h	51.9 b-f	52.7 g-i
PI 497517	-1.6 a	-3.4 a	0.5	cd	0.8 a	34.9 c-g	39.3 a-g	0.70 a	0.73 a	11.6 j,k	29.2 c-g	0.28 h	0.86 a	5.4 i-k	14.6 a	3552 c-f	6820 a	65.2 a	72.0 b-e	59.9 a-f	48.4 h-k
PI 494018	-3.2 a	-2.5 a	0	d	0.6 a	34.4 e-g	42.2 a-f	0.68 a	0.66 a	14.7 g-j	28.8 d-g	0.35 c-h	0.86 a	6.3 e-j	13.7 a	2148 f,g	5502 a	58.7 a	74.2 a-d	46.4 d-f	33.3 n
PI 493938	-2.4 a	-2.8 a	0.5	cd	1.1 a	37.8 a-f	43.5 a-e	0.68 a	0.73 a	14.1 h-j	28.2 e-g	0.37 c-h	0.80 a	5.8 h-k	13.2 a	2588 d-g	6510 a	66.2 a	69.1 c-h	56.2 b-f	37.4 m,n
PI 493880	-1.8 a	-2.9 a	0	d	0.5 a	40.5 a-e	48.0 a,b	0.68 a	0.68 a	13.7 h-k	32.5 a-c	0.28 h	1.19 a	5.8 h-k	16.6 a	3935 cd	6161 a	66.7 a	69.2 c-h	53.8 b-f	42.5 k-m
PI 493729	-2.6 a	-2.6 a	0	d	0.9 a	34.5 e-g	37.7 a-g	0.68 a	0.72 a	12.4 i-k	30.7 b-g	0.29 g,h	0.82 a	5.0 j,k	15.3 a	2832 d-g	5173 a	67.5 a	69.8 b-h	61.5 a-e	41.7 k-m
C7616	-3.1 a	-2.8 a	0	d	0.4 a	41.4 a	27.8 g	0.68 a	0.76 a	21.1 a-d	31.7 a-d	0.55 a,b	1.40 a	8.5 a,b	16.2 a	4753 b,c	6200 a	66.5 a	70.1 b-h	55.0 b-f	71.1 d,e
Mean	-2.4	-3.1	0.3	0.6	38.4	38.3	0.68	0.71	17.3	31.1	0.4	1.0	6.7	15.4	3128	5720	65.0	70.2	56.4	57.0	
<i>p</i> -Value	0.854	0.38	0.001	0.853	0.002	0.003	0.928	0.073	<0.0001	0.0016	<0.0001	0.688	<0.0001	0.489	<0.0001	0.483	0.199	0.006	<0.0001	<0.0001	

TVOL14—TamVal OL14; TS90—TamSpan 90; TROL11—TamRun OL11; NMVALC—New Mexico Valencia C; CTD—canopy temperature depression; RCC—relative chlorophyll content; SLA—specific leaf area; A—CO₂ assimilation rate; g_s—stomatal conductance rate; E—transpiration rate.

Previous studies have documented that peanut plants with high SLAs, i.e., larger, thinner leaves, can lose water through the epidermis and wilt faster than peanut plant with low SLAs and thicker leaves [69]. Such plants may also exhibit severe chlorophyll degradation at low leaf–water potentials [70]. Consequently, it is commonly accepted that greener cultivars with low SLAs are desirable for drought conditions [19]. Among the 28 genotypes that were tested, Wynne, Walton, C76-16, PI 296558, and PI 268996 showed a combination of a higher RCC (>40) and a lower SLA (<33 cm² g⁻¹) compared to the other genotypes when grown under well-watered conditions.

As electrons travel the thylakoid membrane, PS II reaction centers need to be open to initiate photochemistry. This is achieved via plastoquinone Q_A, bound to PS II, which can quickly be re-oxidized to keep the reaction centers open and photochemistry going [71]. However, under stress, light can become very strong so that Q_A⁻ re-oxidation stops and the PS II centers remain closed. In this case, excess energy is dissipated via chlorophyll fluorescence, which can range from 2 to 10% of the absorbed light, depending on the status of the PS II and the carbon assimilation rate [72]. The relationship between photosynthesis and the intensity of the chlorophyll fluorescence has been well documented for decades [73]. Chlorophyll fluorescence has since been used to detect herbicidal injuries and responses to abiotic stresses [74–77]. In 2019, in the well-watered regime, there were no significant differences among the genotypes for the PS II quantum yield, and both the dark- and light-adapted fluorescences averaged around 0.7, which are expected values for healthy plants in the field. However, significant differences among the genotypes were noted for A in both years and for g_s and E in 2018, suggesting that in Virginia's coastal environment, peanut photosynthesis may be more responsive to gas exchange processes rather than electron transport (Table 2). The genotypic averages in 2018 were 17 μmol m⁻² s⁻¹ for A, 0.4 mol m⁻² s⁻¹ for g_s, and 6.7 mmol m⁻² s⁻¹ for E. These were approximately half the values recorded in 2019, a year with better conditions for a high peanut yield. Cultivars Walton (6915 kg ha⁻¹ in 2018 and 6549 kg ha⁻¹ in 2019) and Wynne (6276 kg ha⁻¹ in 2018 and 6122 kg ha⁻¹ in 2019) and the drought-tolerant check C76-16 (4753 kg ha⁻¹ in 2018 and 6200 kg ha⁻¹ in 2019) consistently produced high pod yields in both years. In addition, they also had higher-than-average A, g_s, and E values in both years. New Mexico Valencia C produced not only the highest pod yield in 2019 (6975 kg ha⁻¹) but also the lowest yield in 2018 (1628 kg ha⁻¹). The genotypes TamRun OL11, Walton, and PI 162655 had outstanding shelling percentages, above 70% in both years. Significant differences among the genotypes for the 100-seed weight existed within each year, but the year had a significant effect on individual genotypes even in the well-watered regime.

3.3. Morpho-Physiological and Agronomic Characteristics in the Drought Regime

Under drought conditions, there were no significant differences in the CTD among the genotypes, and, on average, plants were hotter in the drought regime than in the well-watered regime. As a result, wilting was more pronounced, and significant genotypic differences for wilting scores were observed in 2019. The mean CTDs among all the genotypes were -1.0 °C in 2018 and 1.3 °C in 2019, and the average wilting score was >2.0 in both years (Table 3). Some genotypes showed wilting scores above 3, indicating severe wilting, with leaves changing color because of chlorophyll degradation; visible bare ground; and some leaves becoming dried and crisped. Drought-tolerant check C76-16 and TamVal OL 14 along with PIs 476636, 478819, 157542, 298854, and 493880 had the coolest canopies and were the least wilted in both years. C76-16, TamVal OL 14, and PIs 476636, 478819, and 493880 were also among the highest yielding genotypes. There were no significant differences among the genotypes for the SLA, but differences in the RCC were observed in both years, with a noticeable negative relationship between wilting and the RCC. Previous studies on drought-affected peanuts have demonstrated that reduced stomatal conductance due to drought stress negatively influences photosynthesis, altering leaf pigments, like chlorophyll [78]. This results in decreased RCCs and could explain the decrease in the RCC as wilting increases. There were no significant differences among the genotypes for the PS

II quantum yield among the genotypes under drought conditions. Although the genotypic averages were significantly lower under drought conditions (0.64 for light-adapted and 0.69 for dark-adapted quantum yields) than in the well-watered regime, the PS II quantum yield values were above 0.60, as considered by Ritchie (2006) [49], the threshold where PS II is less operational under stress. However, there were a few exceptions. For example, cultivar New Mexico Valencia C and PIs 339960 and 493729 had light-adapted quantum yield values of ≤ 0.57 . Under the same conditions, the drought-tolerant check C76-16 and PI 317968 exceeded 0.70 for the light- and dark-adapted quantum yields in both years. Significant differences among the genotypes for A, g_s , and E values were observed in both years, with genotypic averages of $15.1 \mu\text{mol m}^{-2} \text{s}^{-1}$ for A, $0.2 \text{ mol m}^{-2} \text{s}^{-1}$ for g_s , and 3.8 to 6.1 $\text{mmol m}^{-2} \text{s}^{-1}$ for E, values which are noticeably lower than those for the well-watered regime (Table 3). The pod yield, shelling percentage, and 100-seed weight were also significantly lower under drought conditions than in the well-watered regime, and significant differences among the genotypes were observed for all these traits.

3.4. Relationships among Characteristics

Leaf wilting significantly reduced A ($R^2 = 0.77$), the PS II quantum yield ($R^2 = 0.28$), and the pod yield ($R^2 = 0.66$), while the SLA increased ($R^2 = 0.39$) (Figure 2). The pod yield was significantly associated with A ($R^2 = 0.65$) and the PS II quantum yield ($R^2 = 0.24$), i.e., less wilting, a higher A value and quantum yield, and a higher pod yield.

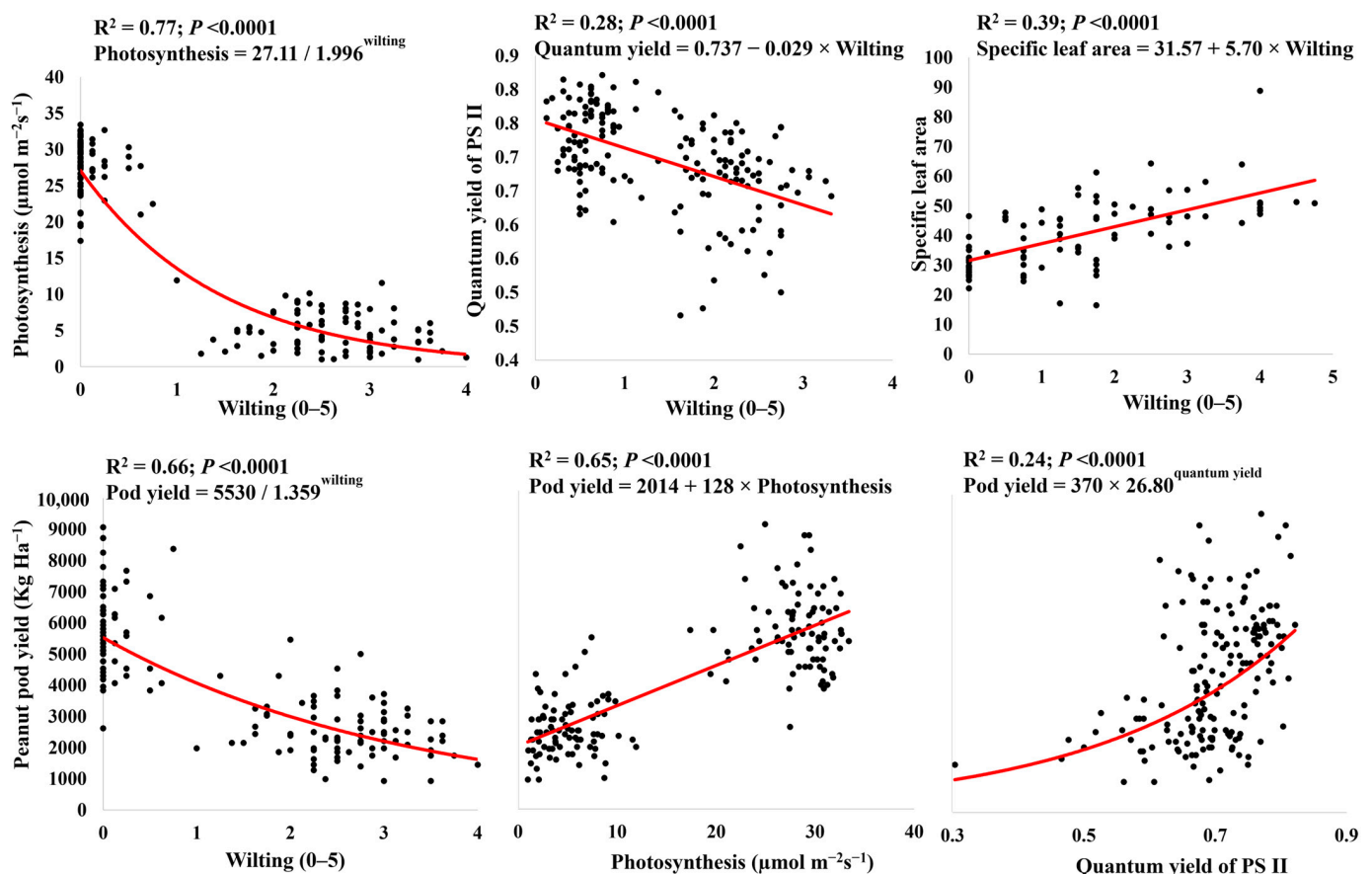


Figure 2. Relationships between physiological characteristics and yield for peanuts grown in two water regimes: drought and well-watered. Each data point represents the genotypes and water regimes averaged across replicates.

Table 3. Growth and yield characteristics of 28 U.S. peanut mini-core and check genotypes grown under drought conditions (rainout shelters) in 2018 and 2019. The values indicated by the same letters are not significantly different using LS means adjusted for Student’s *t* test at $\alpha = 0.05$.

Genotype	CTD (°C)		Wilting (0–5)		RCC	SLA (cm ² g ^{−1})	PS II Quantum Yield (2019)		A (μmol m ^{−2} s ^{−1})		g _s (mol m ^{−2} s ^{−1})		E (mmol m ^{−2} s ^{−1})		Pod Yield (kg ha ^{−1})		Shelling (%)		100-Seed Weight (g)		
	2018	2019	2018	2019	2018	2018	Light	Dark	2018	2019	2018	2019	2018	2019	2018	2019	2018	2019	2018	2019	
Wynne	0.4 a	1.0 a	3.0 a	2.2 a–f	42.2 a–d	30.2 a	0.66 a	0.70 a	17.4 a–g	15.6 a–e	0.25 a–c	0.38 a	5 a–c	6.4 a	2050 b–e	3410 a–c	66.1 a–d	60.4 g–i	50.7 b–e	96.0 a	
Walton	−0.4 a	1.3 a	2.4 a	1.5 F	42.0 a–e	35.1 a	0.68 a	0.72 a	17.8 a–f	13.4 c–e	0.25 a–c	0.24 a	4.9 a–d	6.9 a	3462 a	2868 a–g	61.5 c–h	73.8 a	43.9 d, e	79.7 b, c	
TVOL14	−2.2 a	1.7 a	1.6 a	2.1 b–f	35.4 e–l	39.2 a	0.65 a	0.70 a	15.1 d–j	13.1 d, e	0.14 e–h	0.06 a	3.4 e–j	5.7 a	1777 c–h	3197 a–d	57.6 f–i	62.1 f, g	43.4 d, e	48.1 h–j	
TS90	−1.5 a	1.2 a	3.2 a	1.9 d–f	39.5 a–h	44.1 a	0.65 a	0.71 a	13.9 g–l	15.3 a–e	0.14 e–h	0.05 a	3.3 f–j	6.7 a	1695 c–h	3100 a–e	67.1 a–d	67.7 a–f	54.6 a–e	42.3 j–n	
TROL11	0.6 a	1.9 a	3.6 a	2.9 A	42.1 a–e	36.7 a	0.64 a	0.68 a	14.7 e–l	13.5 c–e	0.14 e–h	0.11 a	3.4 f–j	5.3 a	1964 b–g	2286 b–g	72.9 a	64.8 b–g	49.7 b–e	52.1 g, h	
NMVALC	−1.1 a	1.4 a	3.0 a	2.6 a–c	31.4 j–l	37.3 a	0.53 a	0.60 a	12.7 h–l	15.2 a–e	0.11 f–h	0.15 a	2.7 g–j	5.3 a	1065 d–i	2364 a–g	61.6 c–h	66.3 b–g	56.9 a–e	43.3 i–l	
PI 323268	0.6 a	1.2 a	3.2 a	2.3 a–f	40.3 a–g	35.3 a	0.71 a	0.69 a	17.8 a–f	15.5 a–e	0.22 a–e	0.21 a	4.5 a–f	6.3 a	1573 c–i	2887 a–g	55.8 g–i	54.8 h–j	49.9 b–e	62.6 e, f	
PI 476636	−1.0 a	1.6 a	1.8 a	2.2 a–f	44.4 a	32.2 a	0.62 a	0.68 a	19.2 a, b	14.9 a–e	0.27 a, b	0.11 a	5.2 a	5.6 a	2259 b, c	3565 a	71.1 a, b	65.8 b–g	46.2 b–e	51.6 g, h	
PI 478819	−1.6 a	1.2 a	1.6 a	1.7 Ef	38.3 a–i	28.6 a	0.64 a	0.69 a	19.1 a–c	18.4 a	0.24 a, b	0.34 a	4.8 a–e	7.5 a	1976 b–f	2887 a–g	64.4 b–f	71.0 a, b	48.7 b–e	57.3 f, g	
PI 403813	−2.0 a	1.5 a	1.7 a	2.8 a, b	30.8 kl	34.7 a	0.59 a	0.64 a	11.5 kl	12.4 e	0.09 h	0.17 a	2.4 i, j	5.6 a	1002 e–i	1938 e–g	63.2 c–g	65.6 b–g	49.6 b–e	36.9 n–p	
PI 157542	0.1 a	1.7 a	1.2 a	1.9 c–f	37.9 a–j	40.5 a	0.68 a	0.72 a	20.1 a	16.6 a–c	0.28 a	0.13 a	5.2 a	7.2 a	1497 c–i	2635 a–g	67.7 a–d	70.2 a–c	58.4 a–e	42.7 i–m	
PI 259836	0.2 a	0.9 a	2.2 a	2.0 c–f	29.1 l	38.1 a	0.67 a	0.73 a	17.0 a–g	15.7 a–e	0.21 a–e	0.03 a	4.3 a–f	7.5 a	1625 c–h	2054 d–g	67.2 a–d	66.1 b–g	53.6 b–e	44.5 i–l	
PI 296558	−1.9 a	1.4 a	2.5 a	1.8 d–f	39.8 a–g	35.9 a	0.67 a	0.72 a	18.3 a–e	14.7 b–e	0.25 a–d	0.27 a	5.0 a, b	5.6 a	1309 c–i	2170 c–g	62.3 c–h	62.8 e–g	59.3 a–d	65.0 d–f	
PI 319768	−0.7 a	1.0 a	3.1 a	2.4 a–e	42.5 a–c	37.1 a	0.73 a	0.71 a	16.1 b–h	14.4 b–e	0.18 a–e	0.18 a	4.0 a–g	5.9 a	900 g–i	1879 e–g	65.9 a–e	65.8 b–g	53.0 b–e	35.8 p, q	
PI 268996	−0.2 a	1.1 a	2.3 a	1.9 d–f	41.6 a–f	35.0 a	0.69 a	0.70 a	15.7 b–j	14.2 b–e	0.17 c–g	0.38 a	3.7 b–i	5.4 a	527 i	2131 d–g	56.7 g–i	60.6 g–i	44.8 c–e	48.7 hi	
PI 162655	−0.4 a	1.2 a	2.8 a	2.3 a–f	33.8 g–l	40.8 a	0.67 a	0.70 a	15.2 d–j	12.6 e	0.15 e–h	0.26 a	3.4 e–j	5.6 a	937 f–i	2383 a–g	69.0 a–c	70.0 a–d	62.9 a–c	42.2 j–n	
PI 298854	−1.5 a	1.6 a	1.7 a	2.2 a–f	40.0 a–g	36.7 a	0.66 a	0.71 a	14.9 e–k	16.6 a–c	0.14 e–h	0.46 a	3.2 f–j	6.6 a	1545 c–i	1996 d–g	53.3 l	54.0 i, j	43.9 c–e	73.9 cd	
PI 343398	−0.8 a	1.3 a	2.4 a	1.6 F	36.4 c–k	33.5 a	0.64 a	0.65 a	15.5 c–j	15.5 a–e	0.18 b–f	0.43 a	3.8 b–h	6.7 a	867 hi	2073 d–g	57.3 f–i	60.3 g–i	50.2 b–e	85.2 a, b	
PI 290594	0.8 a	1.5 a	3.9 a	2.0 c–f	35.6 d–l	35.0 a	0.6 a	0.67 a	13.9 g–l	17.3 a, b	0.16 d–g	0.09 a	3.6 c–j	6.2 a	1168 d–i	1686 g	63.2 c–g	65.0 b–g	53.6 b–e	51.7 g, h	
PI 274193	−0.5 a	1.3 a	3.4 a	2.4 a–e	39.2 a–h	37.1 a	0.63 a	0.70 a	12.2 j–l	13.7 c–e	0.10 g, h	0.27 a	2.8 g–j	5.3 a	734 hi	1783 f, g	58.3 e–i	59.9 g–j	46.8 b–e	54.4 g, h	
PI 339960	−1.3 a	1.2 a	2.8 a	2.4 a–e	36.1 c–k	37.7 a	0.57 a	0.67 a	11.2 l	16.3 a–d	0.08 h	0.16 a	2.3 j	7.1 a	832 hi	2151 d–g	56.6 g–i	61.5 f–h	67.7 a, b	44.4 i–l	
PI 502120	−1.1 a	0.6 a	2.3 a	2.5 a–d	36.6 b–k	39.2 a	0.65 a	0.74 a	14.5 f–l	14.4 b–e	0.16 d–g	0.40 a	3.6 d–j	5.8 a	1565 c–i	3023 a–f	55.4 hi	53.4 j	82.1 a	47.8 h–k	
PI 497517	−1.4 a	1.6 a	2.8 a	2.8 A	32.4 i–l	38.8 a	0.65 a	0.69 a	15.8 b–i	12.7 e	0.20 a–e	0.37 a	4.2 a–f	5.0 a	1769 c–h	2868 a–g	61.1 d–h	66.7 b–g	44.2 d, e	40.7 l–p	
PI 494018	−2.7 a	1.2 a	2.5 a	2.4 a–e	31.3 j–l	46.5 a	0.67 a	0.70 a	12.4 i–l	16.3 a–d	0.09 h	0.24 a	2.6 h–j	6.3 a	1554 c–i	2325 a–g	61.6 c–h	69.4 a–e	48.0 c–e	31.9 q	
PI 493938	−2.6 a	0.7 a	2.7 a	2.4 a–e	32.7 h–l	37.1 a	0.64 a	0.71 a	14.7 f–l	16.3 a–d	0.13 e–h	0.32 a	3.2 f–j	6.1 a	1615 c–h	2809 a–g	62.0 c–h	66.6 b–g	49.4 b–e	36.5 o–q	
PI 493880	−2.1 a	1.6 a	1.9 a	2.0 b–f	35.2 f–l	30.8 a	0.60 a	0.70 a	14.0 g–l	17.3 a, b	0.17 c–g	0.10 a	3.5 d–j	7.0 a	2135 b–d	3449 a, b	64.4 b–f	63.5 c–g	42.2 d, e	41.8 k–o	
PI 493729	−1.8 a	1.1 a	2.6 a	2.4 a–e	30.4 kl	38.0 a	0.55 a	0.67 a	11.5 kl	13.9 b–e	0.10 g, h	0.41 a	2.6 h–j	5.1 a	1182 d–i	1918 e–g	60.5 d–i	63.1 d–g	41.9 e	37.5 m–p	
C7616	−1.1 a	1.2 a	2.3 a	1.8 d–f	43.3 a, b	34.0 a	0.70 a	0.73 a	18.7 a–d	15.0 a–e	0.28 a	0.22 a	5.2 a	5.9 a	2903 a, b	3507 a, b	64.9 b–f	61.2 f–h	48.8 b–e	66.7 d, e	
Mean	−1.0	1.3	2.5	2.2	37.2	36.6	0.64	0.69	15.4	15.0	0.2	0.2	3.8	6.1	1553	2548	62.5	64.0	51.6	52.2	
p-Value	0.473	1	0.146	0.009	<0.0001	0.625	0.235	0.477	<0.0001	0.0462	<0.0001	0.068	<0.0001	0.166	0.0003	0.05	<0.0001	<0.0001	<0.0001	<0.0001	<0.0001

TVOL14—TamVal OL14; TS90—TamSpan 90; TROL11—TamRun OL11; NMVALC—New Mexico Valencia C; CTD—canopy temperature depression; RCC—relative chlorophyll content; SLA—specific leaf area; A—CO₂ assimilation rate; g_s—stomatal conductance rate; E—transpiration rate.

Peanut morphological, physiological, and agronomic traits were significantly correlated, positively or negatively, with the aerially derived vegetation indices in both years (Table 4). For example, leaf wilting, and the CTD were highly correlated with the red and blue leaf reflectances, hue, a^* , u^* , GA, GGA, and CSI ($|r| = 0.80\text{--}0.95$). Similarly, gas exchange and electron transport characteristics were significantly correlated with red and green reflectances, NDVI, NPPR, NGRDI, PPR, a^* , u^* , GA, GGA, and CSI ($|r| = 0.60\text{--}0.91$) (Table 4). Previous studies have shown that leaves affected by drought stress exhibit a characteristic wilting behavior, ultimately leading to desiccation without evident chlorosis [34]. In contrast, during instances of disease or nutrient deficiency, leaves tend to display a yellowing discoloration concurrent with wilting, often followed by necrosis before desiccation occurs [79]. This discrepancy in symptomatology underscores the importance for distinguishing between various stressors and their respective impacts on the leaf physiology and appearance. This appearance is crucial when distinguishing drought stress with other stresses using color space indices. The peanut pod yield was the best correlated with NPPR, NGRDI, NCPI, a^* , u^* , GGA, and CSI ($|r| = 0.65\text{--}0.87$). The weakest correlations between ground-based measurements and aerial-image-derived vegetation indices were observed for the RCC, SLA, shelling percentage, and 100-seed weight (Table 4).

Table 4. Correlations of morphological, physiological, and agronomic traits measured for 28 U.S. peanut mini-core and check genotypes grown in drought and well-watered regimes in 2018 and 2019, with ground indices (NDVIs), aerially derived leaf reflectances (red and green), and RGB color indices (hue, a^* , b^* , etc.). The italicized R-values are not significant at a 95% probability.

	CTD		Wilting		RCC	SLA	PSII Quantum Yield		A		g _s		E		Pod Yield		Shelling (%)		100-Seed Wt.	
	2018	2019	2018	2019			Light	Dark	2018	2019	2018	2019	2018	2019	2018	2019	2018	2019	2018	2019
	Red	0.80	0.72	0.90	0.70	-0.47	-0.55	-0.66	-0.74	-0.60	-0.69	-0.80	-0.68	-0.78	-0.67	-0.64	-0.62	-0.38	-0.20	-0.25
Green	0.53	0.34	0.39	0.32	-0.39	-0.29	-0.42	-0.53	-0.42	-0.29	-0.53	-0.28	-0.50	-0.28	-0.46	-0.25	-0.32	0.13	-0.15	-0.63
Blue	0.83	0.77	0.85	0.80	-0.33	-0.47	-0.71	-0.77	-0.59	-0.74	-0.85	-0.75	-0.83	-0.73	-0.67	-0.71	-0.31	-0.25	-0.29	-0.46
NDVI	-0.89	-0.78	-0.94	-0.78	0.21	0.48	0.72	0.75	0.61	0.72	0.88	0.73	0.87	0.72	0.68	0.68	0.27	0.29	0.27	0.55
NPPR	-0.86	-0.91	-0.81	-0.93	0.22	-0.19	0.71	0.75	0.62	0.94	0.89	0.94	0.87	0.94	0.69	0.87	0.30	0.53	0.30	0.40
NGRDI	-0.83	-0.94	-0.83	-0.90	0.32	-0.30	0.69	0.75	0.66	0.92	0.90	0.91	0.89	0.91	0.69	0.82	0.37	0.51	0.29	0.52
PPR	-0.85	-0.75	-0.77	-0.85	0.16	-0.11	0.65	0.65	0.56	0.83	0.85	0.85	0.82	0.84	0.65	0.81	0.25	0.49	0.29	0.01
NCPI	-0.82	0.04	-0.67	-0.17	0.05	0.00	0.11	0.06	0.46	0.11	0.74	0.15	0.71	0.13	0.57	0.20	0.16	0.10	0.27	-0.35
Hue	-0.86	-0.90	-0.80	-0.86	-0.03	0.41	0.69	0.74	-0.58	-0.62	-0.78	-0.61	-0.76	-0.60	0.68	0.79	0.40	0.47	-0.27	-0.61
Intensity	0.77	0.66	0.72	0.65	-0.50	-0.44	-0.63	-0.72	0.66	0.88	0.86	0.87	0.85	0.87	-0.64	-0.56	-0.37	-0.12	0.26	0.52
Saturation	-0.78	-0.65	-0.89	-0.73	0.07	0.49	0.52	0.50	0.53	0.65	0.82	0.68	0.80	0.67	0.63	0.68	0.22	0.40	0.29	-0.13
Lightness	0.53	0.46	0.42	0.44	-0.51	-0.32	-0.49	-0.59	-0.44	-0.41	-0.54	-0.40	-0.52	-0.40	-0.48	-0.36	-0.35	0.05	-0.19	-0.63
a^*	0.88	0.94	0.92	0.94	0.16	-0.45	-0.69	-0.69	-0.63	-0.94	-0.90	-0.94	-0.88	-0.93	-0.67	-0.87	-0.31	-0.61	-0.30	-0.30
b^*	-0.74	-0.42	-0.87	-0.49	-0.18	0.43	0.26	0.19	0.47	0.44	0.76	0.48	0.74	0.47	0.56	0.49	0.16	0.46	0.26	-0.59
u^*	0.89	0.95	0.90	0.93	0.02	-0.44	-0.71	-0.73	-0.65	-0.93	-0.90	-0.93	-0.89	-0.93	-0.68	-0.86	-0.35	-0.56	-0.30	-0.46
v^*	-0.68	-0.33	-0.82	-0.39	-0.29	0.38	0.16	0.07	0.43	0.36	0.70	0.39	0.69	0.38	0.50	0.40	0.12	0.47	0.24	-0.63
GA	-0.79	-0.80	-0.78	-0.81	0.07	0.44	0.69	0.72	0.63	0.74	0.84	0.74	0.82	0.73	0.67	0.73	0.39	0.36	0.24	0.43
GGA	-0.82	-0.93	-0.78	-0.89	0.41	0.42	0.71	0.75	0.65	0.92	0.85	0.91	0.84	0.91	0.64	0.83	0.36	0.49	0.30	0.53
CSI	0.81	0.93	0.76	0.89	-0.43	-0.41	-0.71	-0.75	-0.64	-0.92	-0.83	-0.91	-0.82	-0.91	-0.62	-0.83	-0.36	-0.49	-0.29	-0.53

Values in italics are not significant at $p < 0.05$. CTD—canopy temperature depression; RCC—relative chlorophyll content; SLA—specific leaf area; A—CO₂ assimilation rate; g_s—stomatal conductance rate; E—transpiration rate; Leaf VPD—vapor pressure deficit at the leaf’s surface; NDVI—normalized difference vegetation index; GA—green area; GGA—greener area; CSI—crop senescence index.

3.5. Heritability and Model Development

Similar with findings by our group and others, H² was, in general, higher for the image-derived vegetation indices than for the yield and the manually measured, ground-based morpho-physiological traits [80,81]. This is probably because direct measurements are usually taken from small areas with few leaves from a few plants per plot, whereas aerial images include all the plants and all the visible leaves within each plot. For some of the vegetation indices, H² was high regardless of the water regime, implying that selection may be performed in years with adequate precipitation as well as in dry years. This is important for peanut breeders on the east coast, where precipitation is unpredictable, and irrigation may be unavailable. For example, H² for the crop yield was 0.54 under drought and 0.25 under well-watered conditions (Table 5). The ground-based morpho-physiological

traits measured manually, such as the CTD, wilting, SLA, and gas exchange characteristics, were also as high in H^2 in only one water regime. The few exceptions to this trend, i.e., the RCC and PS II quantum yield, were collected only in one year. In contrast, several vegetation indices collected aurally showed significantly higher H^2 values than ground-based, manually measured traits, with high values in both water regimes. Red and green reflectances, NGRDI, hue, GGA, and CSI had H^2 values from over 0.50 to 0.87, regardless of the water regime. Thus, the estimation of morpho-physiological traits from drone images rather than direct, ground-based measurements may be more useful when working with large breeding populations. With aerial images, many measurements with high H^2 values can be collected relatively quickly and at multiple times during the season. At the farm level, leveraging this understanding through the utilization of drones and remote sensing enables growers to achieve faster and more accurate estimations of the crop health. These methods provide spatiotemporally accurate information, facilitating rapid and precise decision-making regarding resource allocation and management strategies. Thus, embracing drones and remote sensing represents a foundational step toward implementing precision farming practices. However, our study utilized small experimental plots, and extrapolating our findings to a farm-level context would necessitate further investigation. Satellite imagery presents a promising avenue for farm-level analysis because of its capacity to capture imagery over vast acreages. Our results are particularly pertinent for plant breeding studies that demand high-resolution imagery, given our small plot sizes (e.g., 2.13 m × 1.83 m) and the spatial resolution of 0.6 cm utilized in our study.

Table 5. Heritability of morphological, physiological, and agronomic traits measured for 28 U.S. peanut mini-core and check genotypes grown in drought-stressed and well-watered regimes in 2018 and 2019, with leaf spectral reflectances (red, green, and blue); spectral indices (NDVI, NPPR, NGRDI, PPR, and NCPI); and RGB color indices (hue, a*, b*, etc.). Heritability values range from 0 to 1; the closer the values are to 1, the higher the heritability. The colors shift from bright green to bright red as the heritability decreases.

	Drought Stressed	Well-Watered
CTD	0.09	0.67
Wilting	0.20	0.91
RCC	0.67	0.82
SLA	0.20	0.73
PSII Quantum yield (light)	0.72	0.63
PSII Quantum yield (dark)	0.67	0.49
Transpiration	0.17	0.03
Photosynthesis	0.62	0.06
Conductance	0.63	0.09
Yield	0.54	0.25
Shelling	0.90	0.87
100-seed weight	0.82	0.93
Red	0.84	0.80
Green	0.82	0.67
Blue	0.70	0.52
NDVI	0.40	0.43
NPPR	0.51	0.48
NGRDI	0.80	0.59
PPR	0.27	0.66
NCPI	0.17	0.66
Intensity	0.83	0.69
Hue	0.77	0.50
Saturation	0.21	0.66
Lightness	0.78	0.72
a*	0.35	0.24
b*	0.36	0.90
u*	0.66	0.35
v*	0.49	0.81
GA	0.56	0.11
GGA	0.87	0.52
CSI	0.85	0.56

To estimate the gas exchange characteristics, we used forward stepwise regression. Three models, based on the vegetation indices NPPR, hue, a^* , u^* , GA, GGA, and CSI, were identified as the most efficient to estimate A ($R^2 = 0.76$), E ($R^2 = 0.86$), and g_s ($R^2 = 0.86$) (Figure 3). These models, based on the sum of these predictors, are shown below.

$$A = 5.93 - 34.43 \times \text{NPPR} - 0.62 \times \text{Hue} - 1.05 \times a^* + 87.65 \times \text{GGA} + 0.47 \times \text{CSI} \quad (5)$$

This model had $R^2 = 0.76$, RMSE = 4.01, AIC = 637.95, BIC = 655.9, and ASE = 15.2.

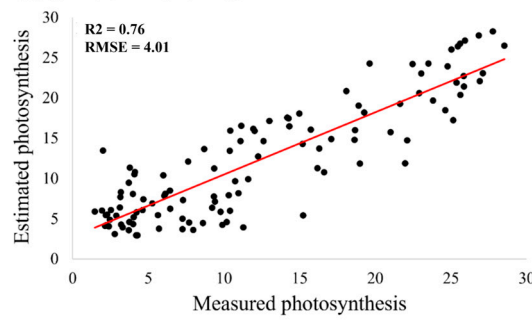
$$E = 1.76 \times u^* + 12.3 \times \text{GA} + 109.29 \times \text{GGA} + 0.73 \times \text{CSI} - 46.31 \times \text{NPPR} - 0.37 \times \text{Hue} - 2.42 \times a^* - 51.89 \quad (6)$$

This model had $R^2 = 0.86$, RMSE = 2.46, AIC = 531.03, BIC = 553.73, and ASE = 5.62.

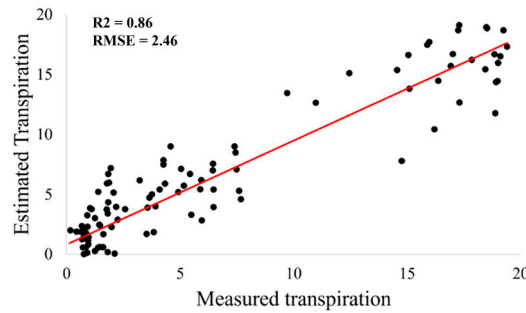
$$g_s = 0.2 - 0.92 \times \text{NPPR} - 0.01 \times \text{Hue} - 0.09 \times a^* + 0.07 \times u^* + 0.39 \times \text{GA} + 1.1 \times \text{GGA} \quad (7)$$

This model had $R^2 = 0.86$, RMSE = 0.089, AIC = -211.74, BIC = -191.39, and ASE = 0.008.

$$\begin{aligned} \text{Photosynthesis} = & 5.93 - 34.43 \times \text{NPPR} - 0.62 \times \text{Hue} - 1.05 \times a^* \\ & + 87.65 \times \text{GGA} + 0.47 \times \text{CSI} \end{aligned}$$



$$\begin{aligned} \text{Transpiration} = & 1.76 \times u^* + 12.3 \times \text{GA} + 109.29 \times \text{GGA} + 0.73 \\ & \times \text{CSI} - 46.31 \times \text{NPPR} - 0.37 \times \text{Hue} - 2.42 \times a^* - 51.89 \end{aligned}$$



$$\begin{aligned} \text{Conductance} = & 0.2 - 0.92 \times \text{NPPR} - 0.01 \times \text{Hue} - 0.09 \times a^* + 0.07 \\ & \times u^* + 0.39 \times \text{GA} + 1.1 \times \text{GGA} \end{aligned}$$

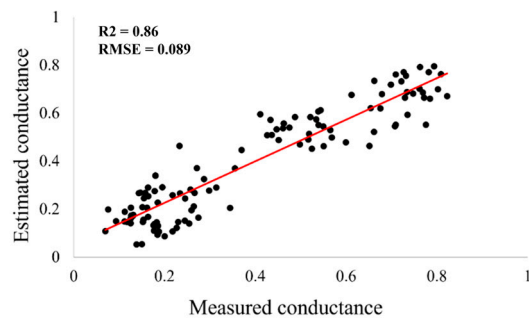


Figure 3. Comparison of manually measured CO_2 assimilations, stomatal conductances, and transpiration rates and rates derived from the vegetation indices collected aerially. The models that best fit the combined data from 2018 and 2019 under drought and well-watered conditions are presented at the top of each figure, with the coefficient of determination (R^2) showing the efficiency of the model.

4. Conclusions

This study evaluated 21 accessions from the US mini-core peanut collection in addition to seven check genotypes under drought and well-watered conditions. Yield attributes and morpho-physiological traits, such as the CTD, RCC, SLA, wilting, A , g_s , E , and PS II quantum yield, were analyzed in response to two water regimes, from direct measurements and aerially derived vegetation indices. We identified several peanut genotypes that performed well in drought and well-watered regimes. These genotypes can be used in breeding to improve drought tolerance through targeted morpho-physiological traits, e.g., the maintenance of the cool canopy under drought conditions, the desired combination of a high RCC and a low SLA, and a high PS II quantum yield and A value under drought conditions. Finally, we identified vegetation indices with high heritability to best estimate the morpho-physiological and agronomic traits that may allow for efficient and more cost-effective selection to improve the drought tolerance of peanut plants.

Supplementary Materials: The following supporting information can be downloaded at <https://www.mdpi.com/article/10.3390/agriculture14040565/s1>, List of 28 genotypes from the U.S. mini-core collection used for this study along with their market and botanical types, and basis for selection including yield, relative chlorophyll content (RCC), number of flowers per plant (Flo), susceptibility to stomatal closure (Clos), susceptibility to wilting (Wilt), canopy temperature (Temp), canopy temperature depression (CTD), normalized difference vegetative index (NDVI). These observations were collected prior to this study in Texas, Oklahoma, and Virginia. For example: the yield column shows which of the genotypes are high, low, or mid-yielding.

Author Contributions: M.B. designed and implemented the experiments, supervised the graduate student in data collection, and wrote the manuscript. S.S. collected and analyzed the data, developed the models, wrote the first draft of the manuscript, and edited the manuscript. R.S.B. and M.D.B. selected the accessions and checks for the study and edited the manuscript. All authors have read and agreed to the published version of the manuscript.

Funding: This study was funded by USDA NIFA-CARE (GRANT12213079) and NIFA-AFRI (GRANT12230636) and by the Virginia Crop Improvement Association (VCIA).

Institutional Review Board Statement: Not applicable.

Data Availability Statement: The data will be available upon request from the corresponding author.

Acknowledgments: The authors would like to thank the sponsors, USDA-NIFA and VCIA; lab technicians Doug Redd, Frank Bryant, and Collin Hoy for their help with tillage operations and the establishment, management, and field data collection of the peanut plots; and T. Isleib for providing seeds of the genotypes used in this study.

Conflicts of Interest: The authors declare no conflicts of interest. Mention of trade names or commercial products in this publication is solely for the purpose of providing specific information and does not imply recommendation or endorsement by the USDA. The USDA is an equal opportunity provider and employer.

References

1. Reddy, M.S. *Dryland Farming Research in Ethiopia Review of the Past and Thrust in the Nineties*; Institute of Agricultural Research: Addis Ababa, Ethiopia, 1993.
2. Stansell, J.; Shepherd, J.; Pallas, J.; Bruce, R.; Minton, N.; Bell, D.; Morgan, L. Peanut responses to soil water variables in the Southeast. *Peanut Sci.* **1976**, *3*, 44–48. [[CrossRef](#)]
3. Pahalwan, D.; Tripathi, R. Irrigation scheduling based on evaporation and crop water requirement for summer peanuts. *Peanut Sci.* **1984**, *11*, 4–6. [[CrossRef](#)]
4. Naveen, P.; Daniel, K.; Subramanian, P.; Senthil Kumar, P. Response of irrigated groundnut (*Arachis hypogaea*) to moisture stress and its management. *Indian J. Agron.* **1992**, *37*, 82.
5. Smartt, J. The groundnut in farming systems and the rural economy—A global view. In *The Groundnut Crop*; Springer: Berlin/Heidelberg, Germany, 1994; pp. 664–699.
6. Rucker, K.; Kvien, C.; Holbrook, C.; Hook, J. Identification of peanut genotypes with improved drought avoidance traits. *Peanut Sci.* **1995**, *22*, 14–18. [[CrossRef](#)]

7. Prasad, P.; Craufurd, P.; Summerfield, R. Sensitivity of peanut to timing of heat stress during reproductive development. *Crop Sci.* **1999**, *39*, 1352–1357. [[CrossRef](#)]
8. Reddy, T.; Reddy, V.; Anbumozhi, V. Physiological responses of groundnut (*Arachis hypogaea* L.) to drought stress and its amelioration: A critical review. *Plant Growth Regul.* **2003**, *41*, 75–88. [[CrossRef](#)]
9. Balota, M. Rainout Shelter-Induced Water Deficit Negatively Impacts Peanut Yield and Quality in a Sub-Humid Environment. *Peanut Sci.* **2020**, *47*, 54–65. [[CrossRef](#)]
10. Skelton, B.J.; Shear, G. Calcium translocation in the peanut (*Arachis hypogaea* L.) 1. *Agron. J.* **1971**, *63*, 409–412. [[CrossRef](#)]
11. Wright, G.; Hubick, K.; Farquhar, G. Physiological analysis of peanut cultivar response to timing and duration of drought stress. *Aust. J. Agric. Res.* **1991**, *42*, 453–470. [[CrossRef](#)]
12. Kulkarni, J.; Ravindra, V.; Sojitra, V.; Bhatt, D. Growth, nodulation and N-uptake of groundnut (*Arachis hypogaea* L.) as influenced by water deficit stress at different phenophases. *Oleagineux* **1988**, *43*, 415–419.
13. Devries, J.; Bennett, J.; Albrecht, S.; Boote, K. Water relations, nitrogenase activity and root development of three grain legumes in response to soil water deficits. *Field Crops Res.* **1989**, *21*, 215–226. [[CrossRef](#)]
14. Wilson, D.M.; Stansell, J.R. Effect of irrigation regimes on aflatoxin contamination of peanut pods. *Peanut Sci.* **1983**, *10*, 54–56. [[CrossRef](#)]
15. Sanders, T.; Cole, R.; Blankenship, P.; Dorner, J. Aflatoxin contamination of peanuts from plants drought stressed in pod or root zones. *Peanut Sci.* **1993**, *20*, 5–8. [[CrossRef](#)]
16. Luis, J.M.; Carbone, I.; Payne, G.A.; Bhatnagar, D.; Cary, J.W.; Moore, G.G.; Lebar, M.D.; Wei, Q.; Mack, B.; Ojiambo, P.S. Characterization of morphological changes within stromata during sexual reproduction in *Aspergillus flavus*. *Mycologia* **2020**, *112*, 908–920. [[CrossRef](#)]
17. Hashim, I.; Koehler, P.; Eitenmiller, R. Tocopherols in runner and Virginia peanut cultivars at various maturity stages. *J. Am. Oil Chem. Soc.* **1993**, *70*, 633–635. [[CrossRef](#)]
18. U.S. Department of Agriculture—National Agricultural Statistics Service. 2020. Available online: <https://quickstats.nass.usda.gov/> (accessed on 1 February 2020).
19. Nigam, S.; Chandra, S.; Sridevi, K.R.; Bhukta, M.; Reddy, A.; Rachaputi, N.R.; Wright, G.; Reddy, P.; Deshmukh, M.; Mathur, R. Efficiency of physiological trait-based and empirical selection approaches for drought tolerance in groundnut. *Ann. Appl. Biol.* **2005**, *146*, 433–439. [[CrossRef](#)]
20. Nigam, S.; Aruna, R. Improving breeding efficiency for early maturity in peanut. *Plant Breed. Rev.* **2008**, *30*, 295–322.
21. Arunyanark, A.; Jogloy, S.; Akkasaeng, C.; Vorasoot, N.; Kesmala, T.; Rao, R.N.; Wright, G.; Patanothai, A. Chlorophyll stability is an indicator of drought tolerance in peanut. *J. Agron. Crop Sci.* **2008**, *194*, 113–125. [[CrossRef](#)]
22. Raju, B.R.; Mohankumar, M.V.; Sumanth, K.K.; Rajanna, M.P.; Udayakumar, M.; Prasad, T.G.; Sheshshayee, M.S. Discovery of QTLs for water mining and water use efficiency traits in rice under water-limited condition through association mapping. *Mol. Breed.* **2016**, *36*, 35. [[CrossRef](#)]
23. Reynolds, M.; Langridge, P. Physiological breeding. *Curr. Opin. Plant Biol.* **2016**, *31*, 162–171. [[CrossRef](#)] [[PubMed](#)]
24. Sreeman, S.M.; Vijayaraghavareddy, P.; Sreevathsa, R.; Rajendrareddy, S.; Arakesh, S.; Bharti, P.; Dharmappa, P.; Soolanayakana, R. Introgression of physiological traits for a comprehensive improvement of drought adaptation in crop plants. *Front. Chem.* **2018**, *6*, 92. [[CrossRef](#)] [[PubMed](#)]
25. Sarkar, S.; Jha, P.K. Is precision agriculture worth it? *Yes, may be. J. Biotechnol. Crop Sci.* **2020**, *9*, 4–9.
26. Rao, N.R.; Talwar, H.; Wright, G. Rapid assessment of specific leaf area and leaf nitrogen in peanut (*Arachis hypogaea* L.) using a chlorophyll meter. *J. Agron. Crop Sci.* **2001**, *186*, 175–182.
27. Farooq, M.; Wahid, A.; Kobayashi, N.; Fujita, D.; Basra, S. Plant drought stress: Effects, mechanisms and management. In *Sustainable Agriculture*; Springer: Berlin/Heidelberg, Germany, 2009; pp. 153–188.
28. Awasthi, R.; Kaushal, N.; Vadez, V.; Turner, N.C.; Berger, J.; Siddique, K.H.; Nayyar, H. Individual and combined effects of transient drought and heat stress on carbon assimilation and seed filling in chickpea. *Funct. Plant Biol.* **2014**, *41*, 1148–1167. [[CrossRef](#)] [[PubMed](#)]
29. Blum, A. Plant water relations, plant stress and plant production. In *Plant Breeding for Water-Limited Environments*; Springer: Berlin/Heidelberg, Germany, 2011; pp. 11–52.
30. Bharadiya, J.P.; Tzenios, N.T.; Reddy, M. Forecasting of crop yield using remote sensing data, agrarian factors and machine learning approaches. *J. Eng. Res. Rep.* **2023**, *24*, 29–44.
31. Omia, E.; Bae, H.; Park, E.; Kim, M.S.; Baek, I.; Kabenge, I.; Cho, B.K. Remote sensing in field crop monitoring: A comprehensive review of sensor systems, data analyses and recent advances. *Remote Sens.* **2023**, *15*, 354. [[CrossRef](#)]
32. Wen, W.; Timmermans, J.; Chen, Q.; van Bodegom, P.M. Evaluating crop-specific responses to salinity and drought stress from remote sensing. *Int. J. Appl. Earth Obs. Geoinf.* **2023**, *122*, 103438. [[CrossRef](#)]
33. Sarkar, S.; Cazenave, A.B.; Oakes, J.; McCall, D.; Thomason, W.; Abbot, L.; Balota, M. High-throughput measurement of peanut canopy height using digital surface models. *Plant Phenome J.* **2020**, *3*, e20003. [[CrossRef](#)]
34. Sarkar, S.; Ramsey, A.F.; Cazenave, A.B.; Balota, M. Peanut leaf wilting estimation from RGB color indices and logistic models. *Front. Plant. Sci.* **2021**, *12*, 658621. [[CrossRef](#)] [[PubMed](#)]
35. Sarkar, S.; Cazenave, A.B.; Oakes, J.; McCall, D.; Thomason, W.; Abbott, L.; Balota, M. Aerial high-throughput phenotyping of peanut leaf area index and lateral growth. *Sci. Rep.* **2021**, *11*, 21661. [[CrossRef](#)]

36. Holbrook, C.C.; Anderson, W.F.; Pittman, R.N. Selection of a core collection from the US germplasm collection of peanut. *Crop Sci.* **1993**, *33*, 859–861. [[CrossRef](#)]
37. Holbrook, C.C.; Dong, W. Development and evaluation of a mini core collection for the US peanut germplasm collection. *Crop Sci.* **2005**, *45*, 1540–1544. [[CrossRef](#)]
38. Puppala, N.; Nayak, S.N.; Sanz-Saez, A.; Chen, C.; Devi, M.J.; Nivedita, N.; Bao, Y.; He, G.; Wright, D.A.; Pandey, M.K.; et al. Sustaining yield and nutritional quality of peanuts in harsh environments: Physiological and molecular basis of drought and heat stress tolerance. *Front. Genet.* **2023**, *14*, 1121462. [[CrossRef](#)] [[PubMed](#)]
39. Bennett, R.S.; Burow, M.D.; Balota, M.; Chagoya, J.; Sarkar, S.; Sung, C.-J.; Payton, M.E.; Wang, N.; Payton, P.; Chamberlin, K.D.; et al. Response to drought stress in a subset of the U.S. peanut mini-core evaluated in Oklahoma, Texas, and Virginia. *Peanut Sci.* **2022**, *23*, 71–87. [[CrossRef](#)]
40. Stalker, H.T. Utilizing Wild Species for Peanut Improvement. *Crop Sci.* **2017**, *57*, 1102–1120. [[CrossRef](#)]
41. Balota, M. Agronomic Recommendations and Procedures. In *Virginia Peanut Production Guide*; Balota, M., Ed.; Virginia Cooperative Extension: Blacksburg, VA, USA, 2018; pp. 7–37.
42. Sarkar, S.; Oakes, J.; Cazenave, A.B.; Burow, M.D.; Bennett, R.S.; Chamberlin, K.D.; Wang, N.; White, M.; Payton, P.; Mahan, J.; et al. Evaluation of the US peanut germplasm mini-core collection in the Virginia-Carolina region using traditional and new high-throughput methods. *Agronomy* **2022**, *12*, 1945. [[CrossRef](#)]
43. Luis, J.M.; Ozias-Akins, P.; Holbrook, C.C.; Kemerait, R.C., Jr.; Snider, J.L.; Liakos, V. Phenotyping peanut genotypes for drought tolerance. *Peanut Sci.* **2016**, *43*, 36–48. [[CrossRef](#)]
44. Garnier, E.; Shipley, B.; Roumet, C.; Laurent, G. A standardized protocol for the determination of specific leaf area and leaf dry matter content. *Funct. Ecol.* **2001**, *15*, 688–695. [[CrossRef](#)]
45. Arief, M.A.A.; Kim, H.; Kurniawan, H.; Nugroho, A.P.; Kim, T.; Cho, B.K. Chlorophyll fluorescence imaging for early detection of drought and heat stress in strawberry plants. *Plants* **2023**, *12*, 1387. [[CrossRef](#)]
46. Jakob, T.; Goss, R.; Wilhelm, C. Activation of diadinoxanthin de-epoxidase due to a chlororespiratory proton gradient in the dark in the diatom *Phaeodactylum tricornutum*. *Plant Biol.* **1999**, *1*, 76–82. [[CrossRef](#)]
47. Strasser, R.; Srivastava, A.; Tsimilli-Michael, M. The fluorescence transient as a tool to characterize and screen photosynthetic samples. In *Probing Photosynthesis: Mechanism, Regulation and Adaptation*; Yunus, M., Pathre, U., Mohanty, P., Eds.; Taylor and Francis: London, UK, 2000; pp. 443–480.
48. Appenroth, K.-J.; Stöckel, J.; Srivastava, A.; Strasser, R. Multiple effects of chromate on the photosynthetic apparatus of *Spirodela polyrrhiza* as probed by OJIP chlorophyll a fluorescence measurements. *Environ. Pollut.* **2001**, *115*, 49–64. [[CrossRef](#)] [[PubMed](#)]
49. Ritchie, G.A. Chlorophyll fluorescence: What is it and what do the numbers mean? In *USDA Forest Service Proceeding RMRS*; Rocky Mount Research Station: Fort Collins, CO, USA, 2006; pp. 34–42.
50. Schindelin, J.; Arganda-Carreras, I.; Frise, E.; Kayning, V.; Longair, M.; Pietzsch, T.; Preibisch, S.; Rueden, C.; Saalfeld, S.; Schmid, B.; et al. Fiji: An open-source platform for biological-image analysis. *Nat. Methods* **2012**, *9*, 676–682. [[CrossRef](#)] [[PubMed](#)]
51. Rueden, C.T.; Schindelin, J.; Hiner, M.C.; DeZonia, B.E.; Walter, A.E.; Arena, E.T.; Eliceiri, K.W. ImageJ2: ImageJ for the next generation of scientific image data. *BMC Bioinform.* **2017**, *18*, 529. [[CrossRef](#)] [[PubMed](#)]
52. Yam, K.L.; Papadakis, S.E. A simple digital imaging method for measuring and analyzing color of food surfaces. *J. Food Eng.* **2004**, *61*, 137–142. [[CrossRef](#)]
53. Trussell, H.J.; Saber, E.; Vrhel, M. Color image processing: Basics and special issue overview. *IEEE Signal Process. Mag.* **2005**, *22*, 14–22. [[CrossRef](#)]
54. Casadesús, J.; Kaya, Y.; Bort, J.; Nachit, M.; Araus, J.; Amor, S.; Ferrazzano, G.; Maalouf, F.; Maccaferri, M.; Martos, V. Using vegetation indices derived from conventional digital cameras as selection criteria for wheat breeding in water-limited environments. *Ann. Appl. Biol.* **2007**, *150*, 227–236. [[CrossRef](#)]
55. Liu, Y.; Mu, X.; Wang, H.; Yan, G. A novel method for extracting green fractional vegetation cover from digital images. *J. Veg. Sci.* **2012**, *23*, 406–418. [[CrossRef](#)]
56. Kipp, S.; Mistele, B.; Schmidhalter, U. Identification of stay-green and early senescence phenotypes in high-yielding winter wheat, and their relationship to grain yield and grain protein concentration using high-throughput phenotyping techniques. *Funct. Plant Biol.* **2014**, *41*, 227–235. [[CrossRef](#)]
57. Zhou, B.; Elazab, A.; Bort, J.; Vergara, O.; Serret, M.; Araus, J.L. Low-cost assessment of wheat resistance to yellow rust through conventional RGB images. *Comput. Electron. Agric.* **2015**, *116*, 20–29. [[CrossRef](#)]
58. Rouse, J.W., Jr.; Haas, R.; Schell, J.; Deering, D. Monitoring vegetation systems in the Great Plains with ERTS. *NASA Spec. Publ.* **1974**, *351*, 309.
59. Tucker, C.J. Asymptotic nature of grass canopy spectral reflectance. *Appl. Opt.* **1977**, *16*, 1151–1156. [[CrossRef](#)] [[PubMed](#)]
60. Metternicht, G. Vegetation indices derived from high-resolution airborne videography for precision crop management. *Int. J. Remote Sens.* **2003**, *24*, 2855–2877. [[CrossRef](#)]
61. Penuelas, J.; Gamon, J.A.; Fredeen, A.L.; Merino, J.; Field, C.B. Reflectance indices associated with physiological changes in nitrogen- and water-limited sunflower leaves. *Remote Sens. Environ.* **1994**, *48*, 135–146. [[CrossRef](#)]
62. Allard, A.W. *Principles of Plant Breeding*; John Wiley & Sons: New York, NY, USA, 1999.
63. Johnson, H.W.; Robinson, H.F.; Comstock, R.E. Estimates of genetic and environmental variability of soybean. *Agron. J.* **1995**, *47*, 314–318. [[CrossRef](#)]

64. Balota, M.; Isleib, T.G.; Tallury, S. Variability for drought related traits of virginia-type peanut cultivars and advanced breeding lines. *Crop Sci.* **2012**, *52*, 2702–2713. [[CrossRef](#)]
65. Chavez, M.M. Thermography to explore plant-environment interactions. *J. Exp. Bot.* **2013**, *64*, 3937–3949. [[CrossRef](#)]
66. Lepikhov, S.B. Canopy temperature depression for drought- and heat stress tolerance in wheat breeding. *Mainstream Technol.* **2022**, *26*, 196–201. Available online: www.bionet.nsc.ru/vogis/ (accessed on 12 February 2024). [[CrossRef](#)]
67. Rebetzke, G.J.; Rattey, A.R.; Farquhar, G.D.; Richards, R.A.; Condon, A.G. Genomic regions for canopy temperature and their genetic association with stomatal conductance and grain yield in wheat. *Funct. Plant Biol.* **2013**, *40*, 14–33. [[CrossRef](#)] [[PubMed](#)]
68. Fukai, S.; Mitchell, J. Role of canopy temperature depression in rice. *Crop Environ.* **2022**, *1*, 198–213. [[CrossRef](#)]
69. Nautiyal, P.; Rachaputi, N.R.; Joshi, Y. Moisture-deficit-induced changes in leaf-water content, leaf carbon exchange rate and biomass production in groundnut cultivars differing in specific leaf area. *Field Crops Res.* **2002**, *74*, 67–79. [[CrossRef](#)]
70. Farooq, M.; Gogoi, N.; Barthakur, S.; Baroowa, B.; Bharadwaj, N.; Alghamdi, S.S.; Siddique, K. Drought stress in grain legumes during reproduction and grain filling. *J. Agron. Crop Sci.* **2017**, *203*, 81–102. [[CrossRef](#)]
71. Schreiber, U.; Bilger, W.; Neubauer, C. Chlorophyll fluorescence as a noninvasive indicator for rapid assessment of in vivo photosynthesis. In *Ecophysiology of Photosynthesis*; Schulze, E.D., Caldwell, M.M., Eds.; Springer: Berlin/Heidelberg, Germany, 1995; p. 100.
72. Trissl, H.-W.; Gao, Y.; Wulf, K. Theoretical fluorescence induction curves derived from coupled differential equations describing the primary photochemistry of photosystem II by an exciton-radical pair equilibrium. *Biophys. J.* **1993**, *64*, 974–988. [[CrossRef](#)] [[PubMed](#)]
73. Kautsky, H.; Hirsch, A. Neue Versuche zur Kohlenstoffassimilation (New experiments on carbon assimilation). *Naturwissenschaften* **1931**, *19*, 964. [[CrossRef](#)]
74. Goltsev, V.N.; Kalaji, H.M.; Paunov, M.; Baba, W.; Horaczek, T.; Mojski, J.; Kociel, H.; Allakhverdiev, S.I. Variable chlorophyll fluorescence and its use for assessing physiological condition of plant photosynthetic apparatus. *Fizologiya Rastanii* **2016**, *63*, 881–907. [[CrossRef](#)]
75. Poudyal, D.; Rosenqvist, E.; Ottosen, C.O. Phenotyping from lab to field—Tomato lines screened for heat stress using F_v/F_m maintain high fruit yield during thermal stress in the field. *Funct. Plant Biol.* **2019**, *46*, 44–55. [[CrossRef](#)]
76. Weber, J.F.; Kunz, C.; Peteinatos, G.G.; Santel, H.-J.; Gerhards, R. Utilization of chlorophyll fluorescence imaging technology to detect plant injury by herbicides in sugar beet and soybean. *Weed Technol.* **2017**, *31*, 523–535. [[CrossRef](#)]
77. Zhang, H.; Ge, Y.; Xie, X.; Atefi, A.; Wijewardane, N.K.; Thapa, S. High throughput analysis of leaf chlorophyll content in sorghum using RGB, hyperspectral, and fluorescence imaging and sensor fusion. *Plant Methods* **2022**, *18*, 60. [[CrossRef](#)]
78. Nabi, R.B.S.; Lee, M.H.; Kim, S.; Kim, J.I.; Kim, M.Y.; Cho, K.S.; Oh, E. Physiological and biochemical responses of diverse peanut genotypes under drought stress and recovery at the seedling stage. *Plant Breed. Biotechnol.* **2022**, *10*, 15–30. [[CrossRef](#)]
79. Chapu, I.; Okello, D.K.; Okello, R.C.O.; Odong, T.L.; Sarkar, S.; Balota, M. Exploration of alternative approaches to phenotyping of late leaf spot and groundnut rosette virus disease for groundnut breeding. *Front. Plant Sci.* **2022**, *13*, 912332. [[CrossRef](#)]
80. Oteng-Frimpong, R.; Karikari, B.; Sie, E.K.; Kassim, Y.B.; Puozaa, D.K.; Rasheed, M.A.; Fonceka, D.; Okello, D.K.; Balota, M.; Burow, M.; et al. Multi-locus genome-wide association studies reveal genomic regions and putative candidate genes associated with leaf spot diseases in African groundnut (*Arachis hypogaea* L.) germplasm. *Front. Plant Sci.* **2023**, *13*, 1076744. [[CrossRef](#)]
81. Sie, E.K.; Oteng-Frimpong, R.; Kassim, Y.B.; Puozaa, D.K.; Adjebeng-Danquah, J.; Masawudu, A.R.; Ofori, K.; Danquah, A.; Cazenave, A.B.; Hoisington, D.; et al. GB-image method enables indirect selection for leaf spot resistance and yield estimation in a groundnut breeding program in Western Africa. *Front. Plant Sci.* **2022**, *13*, 957061. [[CrossRef](#)] [[PubMed](#)]

Disclaimer/Publisher’s Note: The statements, opinions and data contained in all publications are solely those of the individual author(s) and contributor(s) and not of MDPI and/or the editor(s). MDPI and/or the editor(s) disclaim responsibility for any injury to people or property resulting from any ideas, methods, instructions or products referred to in the content.